Structural and electrochemical characterization of fullerene-based surfaces of C-60 mono- or bis-adducts grafted onto self-assembled monolayers

Cecchet, Francesca; Rapino, Stefania; Margotti, Massimo; Da Ros, Tatiana; Prato, Maurizio; Paolucci, Francesco; Rudolf, Petra

Published in:
Carbon

DOI:
10.1016/j.carbon.2006.05.024

Publication date:
2006

Available online at www.sciencedirect.com
ScienceDirect
Carbon 44 (2006) 3014–3021
CARBON
www.elsevier.com/locate/carbon

Structural and electrochemical characterization of fullerene-based surfaces of C_{60} mono- or bis-adducts grafted onto self-assembled monolayers

Francesca Cecchet [a,*], Stefania Rapino [b], Massimo Margotti [b], Tatiana Da Ros [c], Maurizio Prato [c], Francesco Paolucci [b], Petra Rudolf [d]

[a] *LISE, Facultés Universitaires Notre-Dame de la Paix, Namur 5000, Belgium*
[b] *Supr EMat, Dipartimento di Chimica "G. Ciamician" and INSTM, Università degli Studi di Bologna, Italy*
[c] *Dipartimento di Scienze Farmaceutiche, Università di Trieste, Italy*
[d] *Materials Science Centre, Rijksuniversiteit Groningen, The Netherlands*

Received 10 March 2006; accepted 16 May 2006
Available online 10 July 2006

Abstract

Single layers of C_{60} mono- and bis-adducts have been obtained by functionalizing an acid-terminated self-assembled monolayer (SAM) of thiols on gold. X-ray photoelectron spectroscopy demonstrated the grafting onto the SAM by covalent bonding, via the formation of an amide bond, while cyclic voltammetry and electrochemical impedance spectroscopy provided information on the redox properties of the C_{60}-films, as well as on structural characteristics.

Keywords: Fullerene; Chemisorption; X-ray photoelectron spectroscopy; Electrochemical properties

1. Introduction

Fullerene and C_{60} derivatives represent a highly appealing class of molecules for their photo-, electrochemical and physical properties, which can be used for developing new materials or devices, applicable in several areas of biological [1–3] and technological interest [4–8]. The desire to exploit the fullerene properties encouraged the synthesis of different types of functionalized fullerenes [9]. One of the various applications of such molecules concerns the biological domain, where opportunely derivatized fullerenes already demonstrated their usefulness in the DNA photocleavage [10–12], as radiotracers in magnetic resonance or X-ray imaging [13,14], and as drug carriers [15,16]. Obviously, an essential condition for the use of modified fullerenes in a biological environment is that they are soluble in water. One class of water-soluble fullerenes is represented by fullerene mono- or bis-adducts having hydrophilic chains linked to the cage through a pyrrolidine ring [17,18].

Chemical modification of fullerenes is also useful for grafting them onto surfaces [19,20]. In this way fulleropyrrolidine derivatives may play a relevant role in the design of novel molecular electronic devices [21]. A method often used to anchor macromolecular units onto a solid surface is the functionalization of a self-assembled monolayer (SAM) of alkanethiols (see for example [21–33]). The success of SAMs is due to the simplicity of the experimental procedure to prepare the films, their reproducibility and the possibility to create a wide range of surfaces via the incorporation of different groups at the end of the alkyl chains. These end groups allow grafting of various types of molecules onto a surface and serve therefore as a starting point from which to build up more complex molecular architectures. In this work the mono- and bis-adducts were

* Corresponding author. Tel.: +32 081 72 4714; fax: +32 081 72 4707.
E-mail address: francesca.cecchet@fundp.ac.be (F. Cecchet).

0008-6223/$ - see front matter © 2006 Elsevier Ltd. All rights reserved.
doi:10.1016/j.carbon.2006.05.024

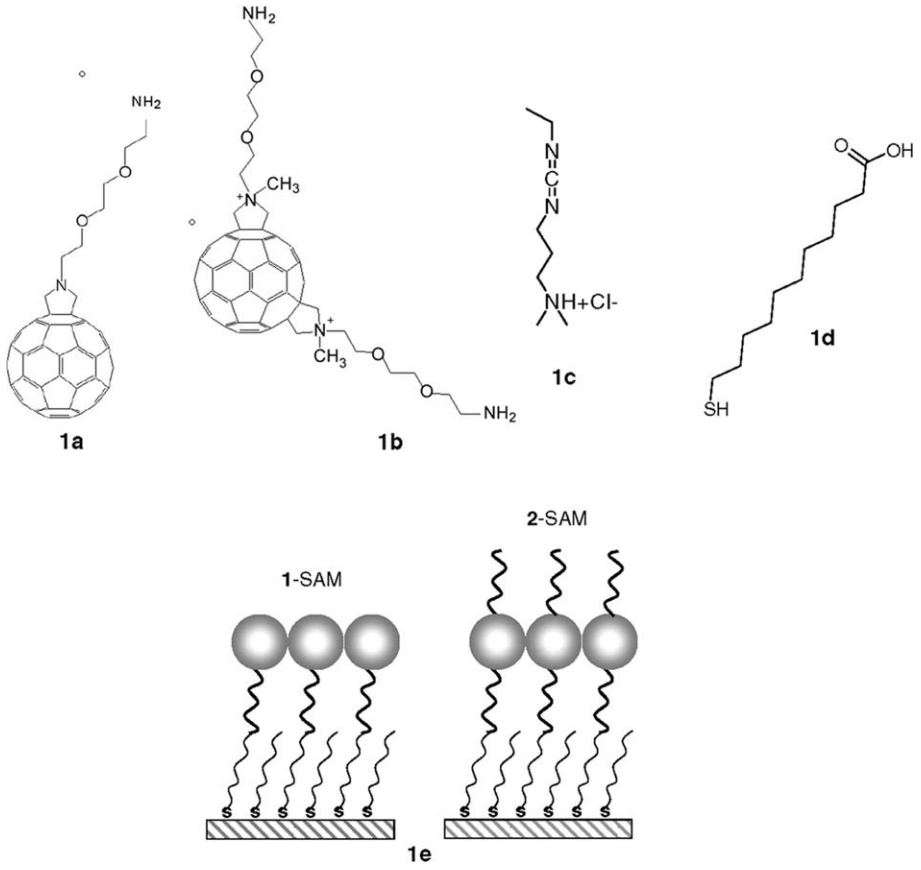

Fig. 1. Representation of (a) mono-derivatized C_{60} and (b) bis-derivatized C_{60} investigated in the present paper; (c) 1-(3-dimethylaminopropyl)-3-ethylcarbodiimide hydrochloride (EDCI), (d) 11-mercaptoundecanoic acid (11-MUA), (e) representation of **1**-SAM and **2**-SAM.

chemically anchored on the surface of an acid-terminated self-assembled monolayer on gold (Fig. 1e) with the aim to investigate the structural and electrical properties of these thin film structures by X-ray photoelectron spectroscopy (XPS), cyclic voltammetry (CV) and impedance spectroscopy (EIS).

2. Experimental

2.1. Materials

Mono- **1** and bis-adduct **2**, schematically shown in Fig. 1a and b, were synthesized as previously reported [18]. The mono-adduct was deprotonated by triethylamine, while bis-derivatized C_{60} molecules were deprotonated in a KOH solution (pH = 11). 1-(3-Dimethylaminopropyl)-3-ethylcarbodiimide hydrochloride (EDCI, 98+% Aldrich) (Fig. 1c), 11-mercaptoundecanoic acid (11-MUA, 95% Aldrich) (Fig. 1d), chloroform and dichloromethane (HPLC grade, Acros) were used as supplied.

2.2. Sample preparation

Evaporated gold films supported on Si(1 1 1) wafers (IMEC, Belgium) were used as substrates in this study. Immediately before being employed they were cleaned in an ozone discharge for 15 min, and sonicated in ethanol for 20 min.

2.2.1. Mono-adduct C_{60} films (**1**-SAM)

We prepared two types of films: a thick bulk-like film of **1** was spin-coated onto the gold surface in atmospheric conditions, using a 1 mM dichloromethane solution of the molecule. The spin-coating equipment was a Specialty Coating Systems (SCS) Model P6700. Single layers of **1** were formed by covalently bonding to carboxylic acid-terminated self-assembled monolayers (SAMs). Carboxylic acid-terminated SAMs were prepared by immersion of the gold substrates in a 1 mM chloroform solution of 11-MUA (11-mercaptoundecanoic acid) for 21 h. The samples were rinsed in chloroform and dried under argon before characterization by XPS (X-ray photoelectron spectroscopy) [34]. For grafting **1** by chemical bonding, the carboxylic acid-terminated SAMs were immersed in a 1 mM dichloromethane solution of EDCI (1-(3-dimethylaminopropyl)-3-ethylcarbodiimide hydrochloride) and **1** for 75 h. EDCI serves as activator for the reaction [23,34]. The modified surfaces were each rinsed and sonicated for 30 s in the pure solvent and dried under a stream of argon prior to analysis by XPS and by electrochemistry.

2.2.2. Bis-adduct C_{60} films (**2**-SAM)

As for **1**, two types of films were prepared with **2**: a thick bulk-like film was deposited on gold by spin-coating, starting from a 1 mM aqueous solution of **2**. Single layers were prepared by chemical bonding to the acid-terminated monolayer of 11-MUA, as described for **1**-SAM films, starting from a 1 mM aqueous solution of EDCI (1-(3-dimethylaminopropyl)-3-ethylcarbodiimide hydrochloride) and **2**. The modified surfaces were each rinsed and sonicated for 30 s in water and dried under a stream of argon prior to analysis by XPS and by electrochemistry.

2.3. Instrumentation

High-resolution X-ray photoelectron spectroscopy (XPS) measurements were performed using a SSX-100 (Surface Science Instruments) photoelectron spectrometer with a monochromatic Al K_α X-ray source ($h\nu = 1486.6$ eV). The energy resolution was set to 0.92 eV and the photoelectron take-off angle (TOA) was 90°. All binding energies were

referenced to the Au4f$_{7/2}$ core level [35]. The base pressure in the spectrometer was in the low 10^{-10} Torr range. Spectral analysis included a linear background subtraction and peak separation using mixed Gaussian–Lorentzian functions, in least squares curve-fitting program (Winspec) developed in the LISE laboratory of the Facultés Universitaires Notre-Dame de la Paix in Namur, Belgium.

Cyclic voltammetry (CV) and electrochemical impedance spectroscopy (EIS) experiments were performed in a 0.1 M tetra-*n*-butylammonium hexafluorophosphate (TBAH) dichloromethane (DCM) solution using a two-compartment electrochemical cell fitted with a saturated calomel electrode (SCE) and a platinum spiral as counter electrode. The reference electrode (Amel, Milan) compartment was separated from that containing the working (surface area ca. 0.5 cm^2) and counter (surface area ca. 5 cm^2) electrodes by a glass frit. Solutions were previously degassed by bubbling Ar through them. CV and EIS experiments were carried out with an Autolab Model PGSTAT 30.

3. Results and discussion

3.1. XPS characterization

Fig. 2 shows the photoemission spectra of the C 1s core level region of 11-MUA monolayer (Fig. 2a), of 11-MUA functionalized with **1** (Fig. 2b) and of 11-MUA functionalized with **2** (Fig. 2c). In the spectrum of 11-MUA SAM (Fig. 2a), the main peak centred at 284.7 eV (**a**) is assigned to the aliphatic carbons of the alkyl chains, the peak at 285.8 eV (**b**) is due to the aliphatic carbon atom bound to the acid group, while the peak at 289.6 eV (**c**) corresponds to the carboxylic carbon atoms [23,36,37]. The spectra recorded for the C_{60} modified 11-MUA SAM surfaces (Fig. 2b and c) show several differences compared to the one recorded for 11-MUA, testifying to the different chemical environments for C atoms in the derivatized C_{60} molecules. Fig. 2b illustrates the mathematical reconstruction of the experimental data recorded for 11-MUA functionalized with **1**: the first peak (**1**) at 285.1 eV contains the contributions from the carbon atoms of the C_{60} cage and from the aliphatic carbon atoms of 11-MUA [23,38]. Peak (**2**) at 285.9 eV corresponds to the aliphatic carbon atoms bound to nitrogen in the chain of **1**. The third peak (**3**), at 287.0 eV, stems from carbon atoms bound to oxygen species in the chain of **1** while feature (**4**) at 289.1 eV can be attributed to unreacted carboxylic carbon atoms of the acid group of 11-MUA. Finally, a shake-up feature associated with the C_{60} cage atoms can be distinguished around 291.0 eV [38]. The C 1s core level spectrum of **2**-SAM (Fig. 2c) clearly testifies to the successful grafting of the molecule on top of the 11-MUA film. In fact, similarly to the analysis carried out for the **1**-SAM, the fitting procedure for this spectrum allows to identify a first peak (**1**) at 285.1 eV which is mainly due to the C_{60} cage atoms but also contains contributions from the aliphatic carbon atoms of 11-MUA; peak (**2**) at 285.8 eV is assigned to carbon atoms bound to nitrogen atoms of the chains of **2**. The spectral signature of carbon atoms bound to oxygen species of the chains of **2** is found at 287.0 eV (**3**): the intensity of this component is more important than the corresponding one in the spectrum of **1**-SAM, because **2** has two identical tails in instead of one. Contribution (**4**) at 289.4 eV is attributed to the unreacted carboxylic carbon atoms of the acid group of 11-MUA and the shake-up feature associated with the C_{60} cage is found around 290.8 eV.

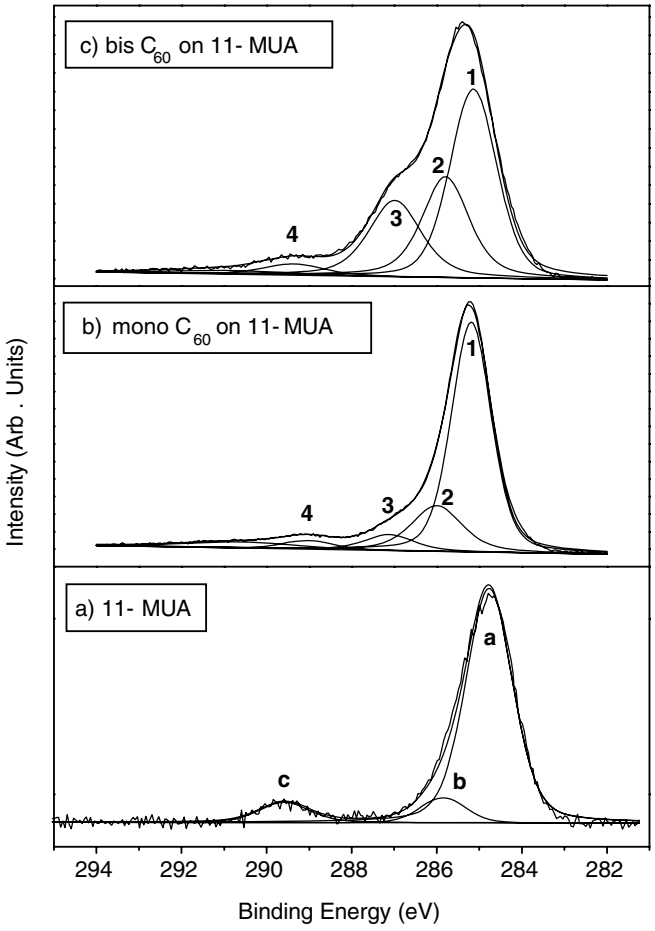

Fig. 2. Photoemission spectra and fit of the C 1s core level region for (a) a film of 11-MUA, (b) a 11-MUA film functionalized with mono-derivatized C_{60} and (c) a 11-MUA film functionalized with bis-derivatized C_{60}.

Figs. 3 and 4 show the photoemission spectra of the N 1s core level of **1**-SAM and **2**-SAM, respectively. The bottom panels in Figs. 3a and b represent the spectra of films prepared by spin-coating. These spin-coated films should be representative of the molecules in a bulk-like phase, where no specific chemical interaction with the substrate is present and where the structure is not influenced by a templating interaction. These spectra give the reference binding energy values of the chemical moieties of the molecules and allow us to identify the binding energy chemical shift of the nitrogen atoms localized at the end of the tails when they are involved in the reaction with the acid groups of 11-MUA.

The spectrum of **1** spin-coated on gold (Fig. 3a, bottom panel) can be reconstructed with two components situated at 399.3 and at 402.3 eV: the first is due to the pyrrolidine nitrogen and to the deprotonated amine nitrogen end of the chain, while the binding energy of the second peak is characteristic of a protonated amine nitrogen [39]. The latter indicates that the starting solution contains **1** in both

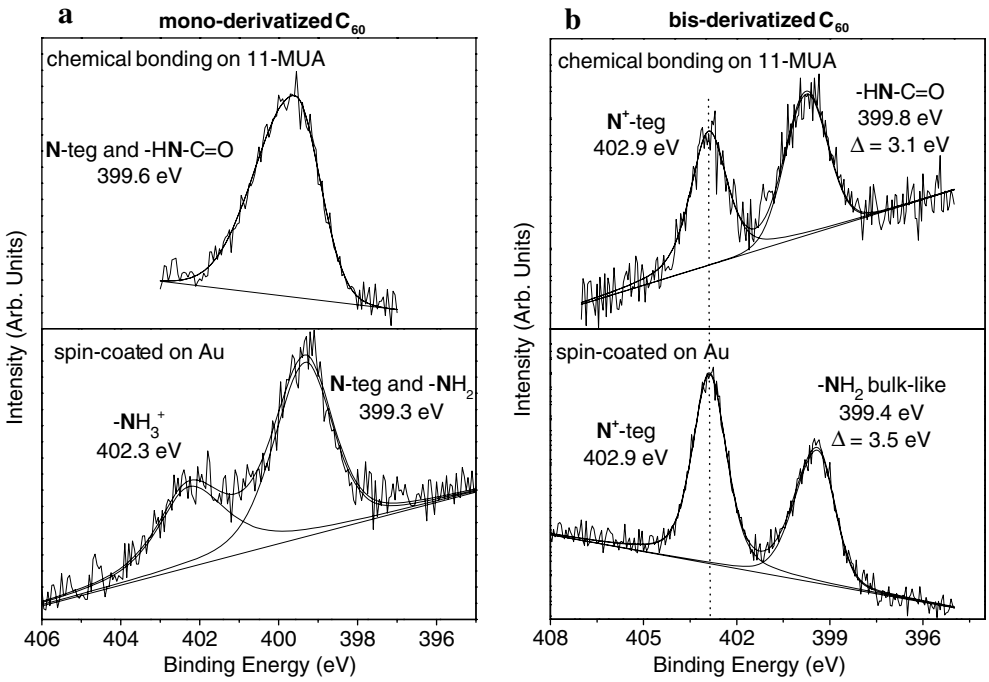

Fig. 3. Photoemission spectra and fit of the N 1s core level region (a) for a spin-coated film of mono-derivatized C_{60} on gold (bottom panel) and a 11-MUA film functionalized with mono-derivatized C_{60} (top panel), and (b) for a spin-coated film of bis-derivatized C_{60} on gold (bottom panel) and a 11-MUA film functionalized with bis-derivatized C_{60} (top panel).

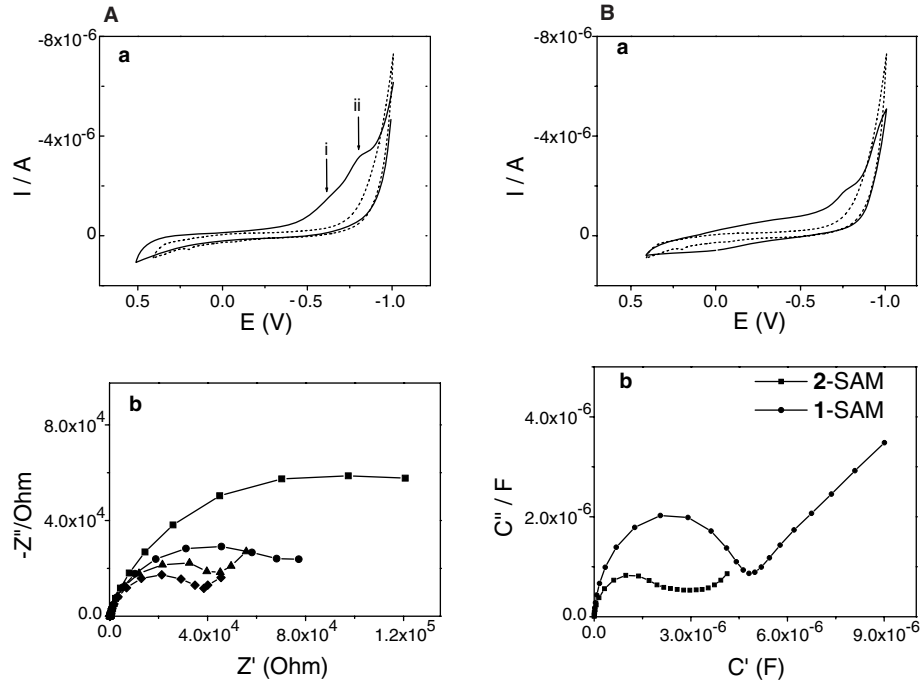

Fig. 4. Part A: (a) cyclic voltammetry curve (full line) of **2**-SAM on gold in 0.1 M TBAH, CH_2Cl_2 solution, scan rate: 20 mV/s. $T = 25$ °C, and of a bare 11-MUA SAM on gold (dashed line); (b) electrochemical impedance spectrum (z-plot, see text) of **2**-SAM on gold in 0.1 M TBAH, CH_2Cl_2 solution. $E = -0.6$ (squares), -0.7 (circles), -0.9 (triangles), -1.0 V (diamonds). Part B: (a) cyclic voltammetry curve (full line) of **1**-SAM on gold in 0.1 M TBAH, CH_2Cl_2 solution, scan rate: 20 mV/s. $T = 25$ °C and of a bare 11-MUA SAM on gold (dashed line); (b) electrochemical impedance spectrum (c-plot, see text) of **2**-SAM (squares) and **1**-SAM (circles) on gold in 0.1 M TBAH, CH_2Cl_2 solution.

forms, protonated and deprotonated, respectively. When **1** is chemically bonded to the acid-terminated self-assembled monolayer, the N 1s photoemission spectrum (Fig. 3a, top panel) does not show the component at higher binding energy and the spectrum is characterized by a main component centred at 399.6 eV, which means that only deproto-

nated **1** are grafted to the surface. The peak is quite large (FWHM = 1.8 eV), with respect to that at 399.3 eV (FWHM = 1.3 eV) of the spin-coated film. This can be explained recalling that the pyrrolidine amine nitrogen is not involved in the bonding to the acid group, while the chain nitrogen atom evolved here into an amide nitrogen environment [39], resulting in the shift to higher binding energy of the latter component and hence the peak broadening. The spectra of **2** spin-coated on gold (Fig. 3b, bottom panel) and of **2**-SAM (Fig. 3b, top panel) give similar information. Both contain a higher binding energy peak, at 402.9 eV, assigned to the N-methylated pyrrolidine nitrogen. In the spin-coated film the lower binding energy contribution at 399.4 eV (FWHM = 1.3 eV) corresponds to the terminal amine nitrogen. However, in the film where the molecules are chemically bonded to the 11-MUA SAM, the lower energy peak is found at 399.8 eV with a FWHM of 1.8 eV, which testifies to the existence of two different chain contributions, the amine nitrogen atom of the unbound tail and the amide nitrogen atoms bound to the acid groups. The latter are characterized by a peak shifted to higher binding energy, and are hence responsible for the broadening of the spectral feature. This data suggests that C_{60} bis-adducts in the **2**-SAM have one of the chains not interacting with underlying surface, and, because of the *trans-2* C_{60} pattern, the free tail probably points out from the surface.

The quantitative analysis of the photoemission spectra allows gaining information on the yield of functionalization of the SAM surface. From the photoemission peak areas we calculated the atomic percentages for each element present in **1**-SAM and **2**-SAM and compared these percentages with the theoretical values expected on the basis of the chemical composition of the films. The error on the photoemission peak areas was estimated depending on the signal-to-noise ratio in the spectrum for each element: the carbon and oxygen signals are well defined and the error was found to be 2% and 5%, respectively. The sulfur and nitrogen signals are weaker, producing a noisier experimental curve, and therefore a more substantial error in the peak area, estimated at 10% and 15%, respectively. To estimate the amount of **1** and **2** grafted onto the SAM surfaces, we considered a model surface of 100% thiol chains and computed the atomic percentages expected for C, O, S and N based on the chemical composition of the molecules, for different coverage of **1** and **2** (i.e. 20%, 25%, 30% of C_{60} adducts on the SAM) as well as the N to S ratio. The latter is obviously related to the grafting yield since nitrogen originates only from C_{60} adducts and sulfur only from 11-MUA. We compared these values with the experimentally determined atomic percentages. In Table 1 we place side by side the experimental percentages for **1**- and **2**-SAM with the theoretical values which correspond best [24]. For **1**-SAM, this comparison indicates that about 25% of the carboxylic groups have reacted with **1** molecules. For **2**-SAM, the comparison indicates that about 30% of the carboxylic groups have reacted with **2** molecules (the attenuation of the S signal by the organic layer has not been taken into account in the calculation and therefore the experimental N/S is probably slightly higher than the real one. However, the 18% error bar estimated for the N/S ratio comprises the systematic error deriving from considering the attenuation of the S signal negligible). The experimental percentages show an excess of oxygen compared to the expected value. The exceeding oxygen may originate from adsorbed water molecules within the films, due to the hydrophilic nature of the C_{60} chains composed of poly(ethylene oxide) units [40]. The higher excess of oxygen for **2**-SAM than for **1**-SAM stems probably from the fact that **2**-SAM surfaces are prepared in water instead of CH_2Cl_2 as done for **1**-SAM.

Table 1
Comparison between experimental atomic percentages derived from the photoemission peak areas of a 11-MUA film functionalized with **1** and **2** and theoretical values calculated for coverages of 25% and 30%, respectively

	1-SAM exp.	**1**-SAM th. 25%	**2**-SAM exp.	**2**-SAM th. 30%
%C	84.1 ± 1.7	87.5	81.1 ± 1.6	86.4
%O	10.2 ± 0.5	7.8	15.5 ± 0.8	8.0
%S	3.9 ± 0.4	3.2	1.6 ± 0.2	2.5
%N	1.8 ± 0.3	1.6	1.8 ± 0.3	3.0
N/S	*0.5 ± 0.1*	*0.5*	*1.2 ± 0.2*	*1.2*

The error on the experimental atomic percentages was estimated to be 2% for C, 5 % for O, 10% for S and 15% for N.

3.2. Electrochemical characterization

The electrochemical characterization of 11-MUA SAMs functionalized with either mono-adduct **1** or bis-adduct **2** was performed by cyclic voltammetry (CV) and electrochemical impedance spectroscopy. In the range between 0.4 and −0.7 V, the voltammetric curves relative to 11-MUA SAM (Fig. 4Aa, dashed line), recorded in DCM/TBAH, display the mostly capacitive and low intensity pattern typical of highly blocked electrodes. As the potential is further decreased, a large increase of the cathodic current is observed that is likely associated to disordering of the SAM and the subsequent increase of both capacitive and background faradaic currents due to permeation of the electrolyte in the film. While such an increase in the cathodic current sets a negative potential limit within which the CV investigation of functionalized SAMs can be performed in the present conditions, it is noticeable that the blocking properties of the film are reversibly recovered upon scanning back the potential to less negative potential. Performing the functionalization of the 11-MUA SAM by **2**, as described in a previous section, brought about a significant change in the voltammetric pattern, i.e. the increase in the faradaic current at $E \leqslant -0.3$ V featuring a shoulder at −0.60 and a peak at −0.80 V (Fig. 4Aa, full line). Fulleropyrrolidines and their pyrrolidinium salts, as most of fullerene derivatives, undergo several reduction processes in the

potential region herein investigated [41,42]. In particular, *trans*-2-bis-triethyleneglycol pyrrolidinium bis-adduct, a species structurally closely related to **2**, undergoes two reversible one-electron reductions at −0.27 and −0.74 V, respectively (in THF solutions). The large negative shift of the reduction processes in **2**-SAM with respect to the model species in solution has likely to be associated to the slow ET kinetics typically experienced by redox couples attached to the electrode surface via long saturated bridges [43]. Notice that, in the present systems, the bridging distance (i.e. number of bonds) between the electrode surface and the redox centre (fullerene) largely exceeds that of similar systems, previously reported, where fullerenes were either covalently [19,44] or non-covalently [45] attached onto gold surfaces. The rise of cathodic current in the CV curve of **2**-SAM (the shoulder **i** at −0.60 V) would then be associated to the first reduction of the fullerene moiety, with an overall negative shift of ~300 mV with respect to model species in THF solution. By contrast, the subsequent reduction (peak **ii** at −0.80 V) would be only shifted, with respect to the model, by less than 100 mV. This is not totally unexpected in view of the observed behavior of 11-MUA SAM at negative potential as above described: disordering of the alkylthiol film induced by such negative potentials would allow a closer approach of fullerene moieties to the electrode surface and then faster electron transfer kinetics [46,47].

Electrochemical impedance spectroscopy (EIS) was used to gather further information about the blocking character of the modified SAM, via the investigation of the fullerene-centred electron transfer kinetics and the evaluation of the double-layer capacitance of the modified electrode, whence the average apparent thickness of the organic layer can be estimated [48,49]. In Fig. 4Ab, the out-of-phase component of the impedance, $-Z''$, plotted vs. the in-phase one, $Z' - Z''$ and Z' being parametric functions of the frequency f (Nyquist plot) – is shown as a function of potential. The incomplete semicircles that rapidly shrink upon increasing overpotential are associated with the slow electron transfer kinetics experienced by the redox probe **2** at the modified electrode. The spectrum obtained under open-circuit conditions was fitted using the CNLS method described by Boukamp [50], giving a value for the charge-transfer resistance of 1.8 kΩ [46].

Confirmation of the above attribution of the faradaic processes in the curve relative to **2**-SAM to fullerene-centred reductions was obtained by comparison with the corresponding CV curve for the SAM modified by pyrrolidine **1** (Fig. 4Ba). Along with a significant increase of the capacitive current over most of the investigated potential range, a cathodic shoulder is observed in such a curve at ~−0.75 V, i.e. 150 mV more negative than the analogous process in **2**-SAM. This is in line with the voltammetric behavior in solution of fulleropyrrolidine vis-à-vis fulleropyrrolidinium mono- and bis-adducts [41]. Alkylation of the nitrogen atom(s) in the fullerene-fused heterocycle, and the ensuing formation of the corresponding pyrrolidinum salt, does, in fact, affect significantly the electron-accepting properties of fulleropyrrolidines, bringing about a positive shift of their reduction potentials. In homogeneous THF solutions, model N-TEG *trans*-2-fulleropyrrolidinium bis-adduct was found to be reduced 170 mV earlier than the corresponding mono-adduct pyrrolidine, i.e. a shift very close to that measured between the corresponding SAMs.

Finally, in Fig. 4Bb, the complex capacitances of **1**- and **2**-SAM, measured at the rest potential, are compared. Complex capacitance is defined as $1/j\omega Z$, where Z is the interface (complex) impedance, $j = \sqrt{-1}$ and ω is the angular frequency ($= 2\pi f$). The *c*-plot emphasizes the interface response at higher frequencies with respect to the *z*-plot [51]. Notice that, in the framework of an equivalent circuit description of the electrochemical interface [52], a semicircle in the *c*-plot corresponds to a series RC (resistor, capacitor) arrangement where R (R_Ω) represents the solution resistance, and C ($= C_{dl}$) the double-layer capacitance. C_{dl} is given by the intercept of semicircle with the real axis. The prominently blocking behaviour of both modified electrodes was evidenced by the semicircle observed in the *c*-plots in the medium-to-high frequency range. The values for the double-layer capacitance of **2**-SAM and **1**-SAM, as obtained by the fitting of the EIS spectra, were 3.1 and 4.4 μF/cm^2, respectively.

As the thickness of the layer is indirectly proportional to its C_{dl} ($C_{dl} = \varepsilon\varepsilon_0/d$ where d is the monolayer thickness and ε the average relative dielectric constant of the monolayer), the EIS results indicate that **2**-SAM is thicker than **1**-SAM. Since XPS showed almost the same functionalization yield of **1**- and **2**-SAM (as discussed before), the higher thickness of **2**-SAM may be ascribed to both a rather compact layer, compared to **1**-SAM, and to the presence of the second tail of **2** which points out from the surface (Fig. 1e).

4. Conclusions

Fullerene mono- and bis-adduct **1** and **2** have been anchored onto self-assembled monolayers of alkylthiols on gold, through the formation of an amide bond between the amine function localized on the chains of the fullerene adducts and the terminal acid group of the alkylthiols, as demonstrated by XPS. CV measurements showed that the redox activity of **1**- and **2**-SAM is still detected even through the SAM probably due to the approach of fullerene moieties to the electrode surface following monolayer disordering at negative potential. Both XPS and EIS indicated that C_{60} bis-adducts **2** were bonded to the surface with one chain, the second remaining free and pointing out from the layer. This conformation of **2**-SAM may lead to the use of such a free bio-compatible chain to link biological species. Previous study demonstrated that the trans-2 bis-adduct does not present haemolytic effects [52] and is poorly cytotoxic on different cell lines [17,52]. The presence of the free chain bearing an amine as terminal group will permit to

conjugate this on biological systems (as enzyme, antibodies, proteins) to produce biosensors.

References

[1] Da Ros T, Prato M. Medicinal chemistry with fullerenes and fullerene derivatives. Chem Commun 1999;8:663–9.

[2] Jensen AW, Wilson SR, Schuster DI. Biological applications of fullerenes. Bioorg Med Chem 1996;4:767–79.

[3] Nakamura E, Tokuyama H, Yamago S, Shiraki T, Sugiura Y. Photocytotoxicity of water-soluble fullerene derivatives. Bull Chem Soc Jpn 1996;69:2143–51.

[4] Prato M. [60]Fullerene chemistry for materials science applications. J Mater Chem 1997;7:1097–109.

[5] Geckeler GE, Samal S. Syntheses and properties of macromolecular fullerenes a review. Polym Int 1999;48:743–57.

[6] Imahori H, Sakata Y. Fullerenes as novel acceptors in photosynthetic electron transfer. Eur J Org Chem 1999:2445–57.

[7] Guldi DM, Prato M. Excited-state properties of C_{60} fullerene derivatives. Acc Chem Res 2000;33:695–703.

[8] Segura JL, Martin N. Functionalized oligoarylenes as building blocks for new organic materials. J Mater Chem 2000;11:2403–35.

[9] Hirsch A. In the chemistry of fullerenes. Stuttgart: Thieme Verlag; 1994 [chapter 4].

[10] Tokuyama H, Yamago S, Nakamura E, Shiraki T, Sugiura Y. Photoinduced biochemical activity of fullerene carboxylic acid. J Am Chem Soc 1993;115:7918–9.

[11] Boutorine AS, Takasugi M, Hélène C, Tokuyama H, Isobe H, Nakamura E. Fullerene-oligonucleotide conjugates: photoinduced sequence-specific DNA cleavage. Angew Chem Int Ed 1994;33:2462–5.

[12] Da Ros T, Bergamin M, Vazquez E, Spalluto G, Baiti B, Moro S, et al. Synthesis and molecular modeling studies of fullerene-5,6,7-trimethoxyindole-oligonucleotide conjugates as possible probes for study of photochemical reactions in DNA triple helices. Eur J Org Chem 2002:405–13.

[13] Cagle DW, Thrash TP, Alford M, Chibante LPF, Ehrhardt GJ, Wilson LJ. Synthesis, characterization, and neutron activation of holmium metallofullerenes. J Am Chem Soc 1996;118:8043–7.

[14] Cagle DW, Kennel SJ, Mirzadeh S, Alford JM, Wilson LJ. In vivo studies of fullerene-based materials using endohedral metallofullerene radiotracers. Proc Natl Acad Sci 1999;96:5182–7.

[15] Nakamura E, Isobe H, Tomita N, Sawamura M, Jinno S, Okayama H. Functionalized fullerene as an artificial vector for transfection. Angew Chem Int Ed Engl 2000;39:4254–7.

[16] Zakharian TY, Seryshev A, Sitharaman B, Gilbert BE, Knight V, Wilson LJ. A fullerene-paclitaxel chemotherapeutic: synthesis, characterization, and study of biological activity in tissue culture. J Am Chem Soc 2005;127:12508–9.

[17] Bosi S, Da Ros T, Spalluto G, Balzarini J, Prato M. Synthesis and anti-HIV properties of new water-soluble bis-functionalized [60]fullerene derivatives. Bioorg Med Chem Lett 2003;13:4437–40.

[18] Bosi S, Feruglio L, Milic D, Prato M. Synthesis and water solubility of novel fullerene bisadduct derivatives. Eur J Org Chem 2003:4741–7.

[19] Gu T, Whitesell JK, Fox MA. Electrochemical charging of a fullerene-functionalized self-assembled monolayer on Au(111). J Org Chem 2004;69:4075–80.

[20] Wang P, Chen B, Metzger RM, Da Ros T, Prato M. Preparation and deposition of stable monolayers of fullerene derivatives. J Mater Chem 1997;12:2397–400.

[21] Higashi N, Takahashi M, Niwa M. Immobilization of DNA through intercalation at self-assembled monolayers on gold. Langmuir 1999;15:111–5.

[22] Azehara H, Mizutani W, Suzuki Y, Ishida T, Nagawa Y, Tokumoto H, et al. Fixation and systematic dilution of rotaxane molecules on self-assembled monolayers. Langmuir 2003;19:2115–23.

[23] Ferretti S, Paynter S, Russell DA, Sapsford KE, Richardson DJ. Self-assembled monolayers: a versatile tool for the formulation of bio-surfaces. Trends Anal. Chem. 2000;19:530–40.

[24] Allara D. Critical issues in applications of self-assembled monolayers. Biosens Bioelectron 1995;10:771–83.

[25] Madoz J, Kuznztzov BA, Medrano FJ, Garcia JL, Fernandez VM. Functionalization of gold surfaces for specific and reversible attachment of a fused β-galactosidase and choline-receptor protein. J Am Chem Soc 1997;119:1043–51.

[26] Blonder R, Willner I, Buckmann F. Reconstitution of apo-glucose oxidase on nitrospiropyran and FAD mixed monolayers on gold electrodes: photostimulation of bioelectrocatalytic features of the biocatalyst. J Am Chem Soc 1998;120:9335–41.

[27] Jordan CE, Frey BL, Kornguth S, Corn RM. Characterization of poly-L-lysine adsorption onto alkanethiol-modified gold surfaces with polarization–modulation Fourier transform infrared spectroscopy and surface plasmon resonance measurements. Langmuir 1994;10:3642–8.

[28] Ostuni E, Yan L, Whitesides GM. The interaction of proteins and cells with self-assembled monolayers of alkanethiolates on gold and silver. Colloids Surf B 1999;15:3–30.

[29] Gooding JJ, Hibbert DB. The application of alkanethiol self-assembled monolayers to enzyme electrodes. Trends Anal Chem 1999;18:525–34.

[30] Patel N, Davies MC, Hartshorne M, Heaton RJ, Roberts CJ, Tendler SJB, et al. Immobilization of protein molecules onto homogeneous and mixed carboxylate-terminated self-assembled monolayers. Langmuir 1997;13:6485–90.

[31] Jiang L, Glidle A, Griffith A, McNeil CJ, Cooper JM. Characterising the formation of a bioelectrochemical interface at a self-assembled monolayer using X-ray photoelectron spectroscopy. Bioelectrochem. Bioenerg. 1997;42:15–23.

[32] Yang HC, Dermody DL, Xu C, Ricco AJ, Crooks RM. Molecular interactions between organized, surface-confined monolayers and vapor-phase probe molecules. 8. Reactions between acid-terminated self-assembled monolayers and vapor-phase bases. Langmuir 1996;12:726–35.

[33] Strither T, Cai W, Zhao X, Hamers RJ, Smith LM. Synthesis and characterization of DNA-modified silicon(111) surfaces. J Am Chem Soc 2000;122:1205–9.

[34] Cecchet F, Pilling M, Hevesi L, Schergna S, Wong JKY, Clarkson GJ, et al. Grafting of benzylic amide macrocycles onto acid-terminated self-assembled monolayers studied by XPS, RAIRS, and contact angle measurements. J Phys Chem B 2003;107:10863–72.

[35] Moulder JF, Stickle WF, Sobol PE, Bomben KD. Handbook of photoelectron spectroscopy. Eden Prairie, MN, USA: Perkin–Elmer Corporation, Physical Electronics Division; 1992.

[36] Czandema AW, King DE, Spauling D. Metal overlayers on organic functional groups of self-organized molecular assemblies. 1. X-ray photoelectron spectroscopy of interactions of Cu/COOH on 11-mercaptoundecanoic acid. J Vac Sci Technol A 1991;9:2607–13.

[37] Vogt AD, Han T, Beebe Jr TB. Adsorption of 11-mercaptoundecanoic acid on Ni(111) and its interaction with probe molecules. Langmuir 1997;13:3397–400.

[38] Maxwell AJ, Brühwiler PA, Nilsson A, Mårtensson N, Rudolf P. Photoemission, autoionization, and X-ray-absorption spectroscopy of ultrathin-film C_{60} on Au(110). Phys Rev B 1994;49:10717–25.

[39] Beamson G, Briggs D. High resolution XPS of organic polymers – the Scienta ESCA database. Chichester, UK: John Wiley & Sons Ltd; 1992.

[40] Desai TA, Sharma S. Nanostructured antifouling poly(ethylene glycol) films for silicon-based microsystems. J Nanosci Nanotechnol 2005;5:235–43.

[41] Carano M, Ceroni P, Da Ros T, Kordatos K, Tomberli V, Paolucci F, et al. Electrochemical properties of soluble fullerene derivatives. Electrochim Acta 2000;46:265–9.

[42] Carano M, Da Ros T, Fanti M, Kordatos K, Marcaccio M, Paolucci F, et al. Modulation of the reduction potentials of fullerene derivatives. J Am Chem Soc 2003;125:7139–44.
[43] Smalley JF, Finklea HO, Chidsey CED, Linford MR, Creager SE, Ferraris JP, et al. Heterogeneous electron-transfer kinetics for ruthenium and ferrocene redox moieties through alkanethiol monolayers on gold. J Am Chem Soc 2003;125:2004–13.
[44] Imahori H, Azuma T, Ajavakom A, Norieda H, Yamada H, Sakata Y. An investigation of photocurrent generation by gold electrodes modified with self-assembled monolayers of C_{60}. J Phys Chem B 1999; 103:7233–7.
[45] Zhang S, Palkar A, Fragoso A, Prados P, de Mendoza J, Echegoyen L. Noncovalent immobilization of C_{60} on gold surfaces by SAMs of cyclotriveratrylene derivatives. Chem Mater 2005;17:2063–8.
[46] Anderson MR, Gatin M. Effect of applied potential upon the in situ structure of self-assembled monolayers on gold electrodes. Langmuir 1994;10:1638–41.
[47] Finklea HO. Electrochemistry of organized monolayers of thiols and related molecules on electrodes. In: Bard AJ, Rubinstein I, editors. Electroanalytical chemistry, vol. 19. New York: Dekker; p. 109–335.
[48] Flink S, van Veggel FCJM, Reinhoudt DN. Sensor functionalities in self-assembled monolayers. Adv Mater 2000;12:1315–28.
[49] Boukamp BAA. Nonlinear least squares fit procedure for analysis of immittance data of electrochemical systems. Solid State Ionics 1986; 20:31–44.
[50] Barsoukov E, MacDonald JR, editors. Impedance spectroscopy, theory, experiment, and applications. New York: Wiley-Interscience; 2005.
[51] Bard AJ, Faulkner LR. Electrochemical methods, fundamentals and applications. New York: Wiley; 2001.
[52] Bosi S, Feruglio L, Da Ros T, Spalluto G, Gregoretti B, Terdoslavich M, et al. Hemolytic effects of water-soluble fullerene derivatives. J Med Chem 2004;47:6711–5.